atmosphere

MDPI

Article

Exploring the Sensitivity of Visibility to $PM_{2.5}$ Mass Concentration and Relative Humidity for Different Aerosol Types

Jiao Wang [1,2], Jianhui Wu [2], Baoshuang Liu [2], Xiaohuan Liu [1], Huiwang Gao [1], Yufen Zhang [2,*], Yinchang Feng [2], Suqin Han [3] and Xiang Gong [4]

[1] Key Laboratory of Marine Environment and Ecology, Ministry of Education, Ocean University of China, Qingdao 266100, China; wangjiao@ouc.edu.cn (J.W.); liuxh1983@ouc.edu.cn (X.L.); hwgao@ouc.edu.cn (H.G.)
[2] State Environmental Protection Key Laboratory of Urban Ambient Air Particulate Matter Pollution Prevention and Control, College of Environmental Science and Engineering, Nankai University, Tianjin 300071, China; envwujh@nankai.edu.cn (J.W.); 8226844@nankai.edu.cn (B.L.); fengyc@nankai.edu.cn (Y.F.)
[3] Tianjin Environmental Meterological Center, Tianjin 300074, China; 1120170168@nankai.edu.cn
[4] School of Mathematics & Physics, Qingdao University of Science and Technology, Qingdao 266042, China; gongxiang@ouc.edu.cn
* Correspondence: zhafox@nankai.edu.cn

Abstract: Fine particle ($PM_{2.5}$) mass concentration and relative humidity (RH) are the primary factors influencing atmospheric visibility. There are some studies focused on the complex, nonlinear relationships among visibility, $PM_{2.5}$ concentration, and RH. However, the relative contribution of the two factors to visibility degradation, especially for different aerosol types, is difficult to quantify. In this study, the normalized forward sensitivity index method for identifying the dominant factors of visibility was used on the basis of the sensitivity of visibility to $PM_{2.5}$ and RH changes. The visibility variation per unit of $PM_{2.5}$ or RH was parameterized by derivation of the visibility multivariate function. The method was verified and evaluated based on 4453 valid hour data records in Tianjin, and visibility was identified as being in the RH-sensitive regime when RH was above 75%. In addition, the influence of aerosol chemical compositions on sensitivity of visibility to $PM_{2.5}$ and RH changes was discussed by analyzing the characteristics of extinction components ($(NH_4)_2SO_4$, NH_4NO_3, organic matter, and elemental carbon) measured in Tianjin, 2015. The result showed that the fitting equation of visibility, $PM_{2.5}$, and RH, separately for different aerosol types, further improved the accuracy of the parameterization scheme for visibility in most cases.

Keywords: visibility; sensitivity; $PM_{2.5}$; RH; aerosol types

Citation: Wang, J.; Wu, J.; Liu, B.; Liu, X.; Gao, H.; Zhang, Y.; Feng, Y.; Han, S.; Gong, X. Exploring the Sensitivity of Visibility to $PM_{2.5}$ Mass Concentration and Relative Humidity for Different Aerosol Types. *Atmosphere* **2022**, *13*, 471. https://doi.org/10.3390/atmos13030471

Academic Editor: Rajasekhar Balasubramanian

Received: 16 January 2022
Accepted: 11 March 2022
Published: 14 March 2022

1. Introduction

Atmospheric horizontal visibility is defined as the distance at which the contrast of a black object with respect to its background is equal to the contrast threshold of human eyesight and is an indicator of atmospheric transparency [1]. Good visibility is a desirable feature of any geographical location, and its importance should be considered [2]. However, many megacities have suffered from air pollution incidents accompanied by a decline in visibility during the past several decades [3–5]. Poor visibility severely affects tourism, transportation, and mental health [6–8].

Visibility degradation is mainly attributed to light scattering and absorption by atmospheric fine particles [9,10]. There is an obvious, negative correlation between visibility and $PM_{2.5}$ concentration [11–14]. A form of power function or exponential function between visibility and $PM_{2.5}$ concentration was observed in many cities [11,15,16]. Notably, when the $PM_{2.5}$ concentration was lower than a certain threshold, visibility increased quickly as the $PM_{2.5}$ concentration declined [11,16–18]. The threshold values of $PM_{2.5}$ vary by city. For example, the threshold corresponding to visibility < 10 km in Beijing, Xi'an, and Shanghai

is 110, 88, and 65 μg/m^3, respectively [11,16,17]. This difference may reduce the reliability of haze event identification when a fixed visibility threshold is employed [19].

Visibility variation shows a clear dependence on relative humidity (RH) also [20,21]. Chen et al. [22] indicated that the decrease in visibility was mainly influenced by RH when RH was >90%. Hygroscopic growth usually increases aerosol extinction coefficients by enlarging the particle size due to the uptake of liquid water. In some other cases, aerosol extinction can be decreased by lowering the refractive index because the refractive index of water is smaller than that of other aerosol components [23]. Positive or negative effects are dictated to a large degree by components [21].

There are complex, nonlinear relationships among visibility, $PM_{2.5}$ concentration, and RH, which are deeply affected by the component composition of particles in addition to the mixing state and size distribution [21,24–26]. The effect of particles and RH on visibility is further complicated by the differences in extinction abilities of particle components [11,27,28]. Water-soluble, inorganic salts (e.g., $(NH_4)_2SO_4$, NH_4NO_3) and carbonaceous (e.g., organic matter (OM), elemental carbon (EC) aerosols are the major extinction components in particles with various, dry extinction efficiencies and hygroscopicities [29,30]. The high content of extinction components in particles can increase the sensitivity of visibility to particle concentration. Similarly, the percentage of hygroscopic components (e.g., $(NH_4)_2SO_4$, NH_4NO_3) in $PM_{2.5}$ affects the sensitivity of visibility to RH [10,24]. The content of extinction components in $PM_{2.5}$ varies obviously by region and period [8,11,25]. For example, the content of major extinction components ($(NH_4)_2SO_4$, NH_4NO_3, OM, and EC) and hygroscopic components ($(NH_4)_2SO_4$ and NH_4NO_3) in $PM_{2.5}$ in Shanghai (83% and 42%) was 1.7 times greater than those in Chengdu (48% and 25%, respectively) [31,32]. Thus, identifying the primary factors influencing visibility is essential.

In most cases, atmospheric visibility is affected by both particle concentration and RH; if it is dominated by particulate matter, the effect of emission reduction measures is obvious, but if it is dominated by RH, the same emission reduction measures may not achieve the expected effect. Many studies were conducted to gain insights into correlations between low-visibility events and influencing factors [13,18,30]. However, the sensitivity of visibility to $PM_{2.5}$, mass concentration, and RH by aerosol type remains unclear.

In predicting and preventing low-visibility events, determining whether the main cause is $PM_{2.5}$ or RH is essential [19,33]. There are some studies focused on the complex, nonlinear relationships among visibility, $PM_{2.5}$ concentration, and RH. However, the relative contribution of the two factors to visibility degradation, especially by aerosol type, was difficult to quantify. Thus, this study attempts to build a method for identifying the dominant factors of visibility on the basis of the sensitivity of visibility to $PM_{2.5}$ and RH changes. A total of 4453 valid hour data records of visibility, $PM_{2.5}$, and RH in Tianjin, 2015, were used to verify and evaluate the method. In addition, aerosols were classified based on the extinction component ($(NH_4)_2SO_4$, NH_4NO_3, OC, EC, fine soil, and sea salt) measured synchronously online to analyze the influence of aerosol chemical compositions on sensitivity of visibility to $PM_{2.5}$ and RH changes.

2. Data and Methods

2.1. The Online Observation of $PM_{2.5}$ Chemical Composition and Meteorological Factors

Tianjin (39°100′ N, 117°100′ E) is in the Beijing-Tianjin-Hebei urban agglomeration. It is adjacent to Bohai Bay and has the largest comprehensive port in northern China, the Tianjin Port. The climate is dominated by continental monsoons with distinct seasonal variation and holds the semi-humid characteristic of warm, temperate zones. Sampling instruments used in this study were installed on the rooftop of the Tianjin Eco-Environmental Monitoring Center, approximately 10 m above ground level. The site was expected to reflect the pollution characteristics of a thickly settled urban district.

The mass concentration of $PM_{2.5}$ was sampled 1 time every 5 min using a particle monitor (TEOM 1405-F, Thermo Fisher Scientific, Waltham, MA, USA) from February to December 2015. The values measured within an hour were averaged to match with

other parameters. The monitor was composed of a filter dynamics measurement system and a tapered element oscillating microbalance mass sensor installed in an individual cabinet. The method detection limit (MDL) was up to 0.1 μg/m^3. The inorganic ions (Ca^{2+}, Na^+, NH_4^+, Cl^-, NO_3^-, and SO_4^{2-}) of $PM_{2.5}$ were synchronously analyzed by an ion-monitoring instrument (AIM URG9000D, Enviro Technology Services, Chapel Hill, NC, USA) with 1 h resolution. The AIM was composed of one particle collection system and two ion chromatographs for anion and cation analyses. The MDLs for Ca^{2+}, Na^+, NH_4^+, Cl^-, NO_3^-, and SO_4^{2-} were 2.3, 0.6, 1.8, 0.2, 0.2, and 0.3 μg/m^3, respectively. The 1 h resolution concentration data of carbon components (OC and EC) in $PM_{2.5}$ were determined by a semi-continuous OC/EC analyzer (Sunset Laboratory Inc., Portland, OR, USA). The analyzer was calibrated monthly using a blank punch of pre-heated quartz fiber filter and standard sucrose solutions (3.2 mgC/mL) for quality control. The MDLs for OC and EC were 0.45 and 0.06 μg/cm^2, respectively. The quartz fiber filter was changed weekly during the analysis.

Relative humidity was measured by a VAISALA WST520 automatic weather station with a time resolution of 5 s. The systematic error of relative humidity measurement was within ±3%. Atmospheric visibility was measured using a Belfort 6000 instrument (Belfort Instrument , Belfort, CA, USA), based on forward scattering with a time resolution of 10 min. The systematic error of atmospheric visibility measurement was less than 10%. The visibility values measured within an hour were averaged to match with other parameters. The hourly concentration data for $PM_{2.5}$, water-soluble ions, carbon species, RH, and visibility simultaneously were designated as one sample. Instrument failure, bad weather, and other factors led to partial data loss or abnormality. Singular values (e.g., abnormally high values, abnormally low values, and values above the instrument limit or with a large relative standard deviation) were removed. Details on the quality control (QC) of observations were provided in studies [34,35]. This study obtained 4453 samples from Tianjin, 2015, after validation with QC procedures.

2.2. Parameterization Scheme of Atmospheric Visibility

Many studies found that there is a negative exponential relationship, as shown in Equation (1) [11,36]. Considering the influence of aerosol hygroscopic growth on visibility, RH was selected as another factor for visibility parameterization. Song et al. [36] found that there was a power relationship between RH and visibility, and the function was combined with Equation (1) to simulate visibility (Equation (2)). Another equation, Equation (3), evolved by multiplying the power function between extinction coefficient and aerosol concentration and the empirically power-exponential function between extinction coefficient and RH [22,37,38]. All variables could be easily acquired; thus, the parameterization was practical.

$$V = f(x) = \mathrm{a} \times \exp(\mathrm{b} \times x) + \mathrm{c} \quad (1)$$

where the visibility is a function of one parameter, $PM_{2.5}$: $f(x)$; V and x are visibility and $PM_{2.5}$ with units of km and μg/m^3, respectively; and parameters a, b, and c are the regression coefficients of the schemes.

$$V = f(x,y) = \mathrm{a} \times \exp(\mathrm{b} \times x) + \mathrm{c} \times y^d + \mathrm{e} \quad (2)$$

where the visibility is a function of two parameters, $PM_{2.5}$ and RH: $f(x,y)$; V, x, and y are visibility, $PM_{2.5}$, and RH with units of km, μg/m^3, and %, respectively; and parameters a, b, c, d, and e are the regression coefficients of the schemes.

$$V = f(x,y) = \mathrm{a} \times x^b \times (1-y)^{c \cdot y} \quad (3)$$

where the visibility is a function of two parameters, $PM_{2.5}$ and RH: $f(x,y)$; V, x, and y are visibility, $PM_{2.5}$, and RH with units of km, μg/m^3, and %, respectively; and parameters a, b, and c are the regression coefficients of the schemes.

2.3. Classification Method of Visibility-Sensitive Regime, Depending on the Sensitivity of Visibility to $PM_{2.5}$ Concentration and RH

To test the sensitivity of visibility to $PM_{2.5}$ concentration and RH, the normalized forward sensitivity index method [19,39,40] was used, shown as Equations (4) and (5). The normalized forward sensitivity index ($K_{V\text{-}R}$) of a variable ($PM_{2.5}$ concentration or RH) to visibility is the ratio of the relative change in the variable to the relative change in the visibility.

$$K_{V-PM2.5} = (|\Delta V_{x_i}|/V_{x_i})/(|\Delta x_i|/x_i) = |\Delta V_{x_i}/\Delta x_i| \times x_i/V_{x_i} \quad (4)$$

where V is visibility with units of km; x is $PM_{2.5}$ with units of $\mu g/m^3$; and y is RH with units of %; x_i is the different level of $PM_{2.5}$ concentrations, $i = 1, 2, 3 \ldots \ldots$ m; Δx_i is the variation of x_i; V_{x_i} is the visibility under the i level of $PM_{2.5}$ concentration; ΔV_{x_i} is the visibility variation caused by Δx_i; and $K_{V-PM2.5}$ is the sensitivity index of visibility under the i level of $PM_{2.5}$ concentration.

$$K_{V-RH} = \left(\left|\Delta V_{y_j}\right|/V_{y_j}\right)/(|\Delta y_j|/y_j) = \left|\Delta V_{y_j}/\Delta y_j\right| \times y_j/V_{y_j} \quad (5)$$

where V, x, and y are visibility, $PM_{2.5}$, and RH with units of km, $\mu g/m^3$, and %, respectively. y_j is the different level of RH, $j = 1, 2, 3 \ldots \ldots$ n; Δy_j is the variation of RH at value y_j; V_{y_j} is the visibility under the j level of RH; ΔV_{y_j} is the visibility variation caused by Δy_j; and K_{V-RH} is the sensitivity index of visibility under the j level of RH.

When the variable is a differentiable function of the parameter, the sensitivity index may be alternatively defined using partial derivatives. There is a functional relationship among visibility, $PM_{2.5}$, and RH, shown as Equations (1)–(3) in this study. $K_{V-PM2.5}$ and K_{V-RH} can be approximately expressed as Equations (6) and (7):

$$|\Delta V_x/\Delta x| \approx |f'_x(x, y)| \quad (6)$$

$$\left|\Delta V_y/\Delta y\right| \approx |f'_y(x, y)| \quad (7)$$

where V is visibility with units of km; x is $PM_{2.5}$ with units of $\mu g/m^3$; and y is RH with units of %; $f(x, y)$ is the parameterization scheme of visibility, $PM_{2.5}$ concentration, and RH obtained in Section 2.2; $f'_x(x, y)$ and $f'_y(x, y)$ are partial derivatives of $f(x, y)$, respectively.

Visibility relative sensitivity index $\Omega_{PM/RH}$ is defined as Equation (8):

$$\Omega_{PM/RH} = K_{V-PM2.5}/K_{V-RH} \quad (8)$$

where $K_{V-PM2.5}$ and K_{V-RH} is the sensitivity index of visibility to $PM_{2.5}$ concentration and RH, respectively; and $\Omega_{PM/RH}$ is the ratio of visibility variation per unit of $PM_{2.5}$ to RH.

When $\Omega_{PM/RH} = 1$, the effects of the concentration of $PM_{2.5}$ and RH on visibility is similar. When the ratio is greater than one, indicating that visibility is more sensitive to $PM_{2.5}$ than RH, visibility is identified as being in the $PM_{2.5}$-sensitive regime. When $\Omega_{PM/RH}$ is lower than 1, the visibility variation caused by the increase in RH is greater than that caused by particle concentration, and visibility is identified as being in the RH-sensitive regime. The classification method of visibility for different control categories was used to identify the main influencing factors by determining the threshold of aerosol mass concentration and RH.

2.4. IMPROVE Equations

In this study, the extinction contribution of the composition of fine particles to visibility degradation was investigated using the Interagency Monitoring of Protected Visual Environments (IMPROVE) equation, an extensively used method for estimating the light extinction coefficient based on aerosol chemical composition [41,42]. Equation (9) is the

revised IMPROVE algorithm in which coarse particulate, NO_2, and Rayleigh scattering were excluded because of the low contributions [42,43].

$$\begin{aligned} B_{ext} \approx\ & 2.2 \times f_S(RH) * [Small(NH_4)_2SO_4] + 4.8 \times f_L(RH) * [Large\ (NH_4)_2SO_4] + \\ & 2.4 \times f_S(RH) * [Small(NH_4)_2SO_4] + 5.1 \times f_L(RH) * [Large(NH_4)_2SO_4] + 2.8 \times [Small\ OM] + \\ & 6.1 \times [Large\ OM] + 10 \times [EC] + 1 \times [Fine\ Soil] + 1.7 \times f_{SS}(RH) \times [Sea\ Salt] \end{aligned} \quad (9)$$

where $[(NH4)_2SO_4]$, $[NH_4NO_3]$, $[OM]$, $[EC]$, $[Fine\ Soil]$, and $[Sea\ Salt]$ are the concentrations of $(NH_4)_2SO_4$, NH_4NO_3, OM (organic matter), EC, fine soil, and sea salt in units of μg/m^3; B_{ext} is the light extinction coefficient of aerosol, Mm^{-1}. The fraction of the fine particle component ($(NH4)_2SO_4$, NH_4NO_3, or OM) that is in the large mode is estimated by dividing the total concentration of the component by 20 μg/m^3. The coefficient of the equation is the dry mass extinction efficiency of each extinction component, which represents the light scattering or absorption extinction coefficient under the unit mass concentration. $f_S(RH)$, $f_L(RH)$, and $f_{SS}(RH)$ is the hygroscopic growth factor of small- and large-mode ammonium salt and sea salt, determined according to the measured RH [42].

Most of the sulfate, nitrate, and organic carbon in the particles are in the form of $(NH_4)_2SO_4$, NH_4NO_3, and OM, respectively [44]. The average equivalent concentrations of NH_4^+, SO_4^{2-}, NO_3^- measured in this study were 0.69, 0.13, and 0.22 μeq/m^3, respectively. There was sufficient NH_4^+ to match SO_4^{2-} and NO_3^-. Therefore, the concentrations of $(NH_4)_2SO_4$ and NH_4NO_3 were reconstructed based on Equations (10) and (11). OM was estimated by multiplying the OC by 1.6, which is suitable for urban aerosol (Equation (12)) [42,45]. Sea salt mass was calculated based on the concentrations of Na^+ and Cl^- (Equation (13)) [44]. Fine soil mass was assumed to be 20 times of that of Ca^{2+} based on previous soil source profiles (Equation (14)) [46–48].

$$[(NH_4)_2SO_4] = 1.29\ \left[SO_4^{2-}\right] \quad (10)$$

where $[SO_4^{2-}]$ and $[(NH_4)_2SO_4]$ are the concentrations of SO_4^{2-} and $(NH_4)_2SO_4$ in units of μg/m^3.

$$[NH_4NO_3] = 1.375\ [NO_{3-}] \quad (11)$$

where $[NO_3^-]$ and $[NH_4NO_3]$ are the concentrations of NO_3^- and NH_4NO_3 in units of μg/m^3.

$$[OM] = 1.6\ [OC] \quad (12)$$

where $[OC]$ and $[OM]$ are the concentrations of OC and OM in units of μg/m^3.

$$[Sea\ Salt] = 1.47\ \left[Na^+\right] + \left[Cl^-\right] \quad (13)$$

where $[Sea\ Salt]$, $\left[Na^+\right]$ and $[Cl^-]$ are the concentrations of *sea salt*, Na^+, and Cl^- in units of μg/m^3.

$$[Fine\ Soil] = 20\ \left[Ca^{2+}\right] \quad (14)$$

where $[Fine\ Soil]$ and $[Ca^{2+}]$ are the concentrations of *fine soil* and Ca^{2+} in units of μg/m^3.

3. Results and Discussion

3.1. Application of Visibility Control Category Classification Method

3.1.1. Quantification of Relationships among Visibility, $PM_{2.5}$ Concentration, and RH in Tianjin, 2015

Visibility varied from 0.3 to 35.0 km, with an average of 12.0 ± 9.1 km, from February to December 2015 in Tianjin. The average mass concentration of $PM_{2.5}$ was 106.0 ± 81.2 μg/m^3, and the average RH was 46 ± 21%. There was a strong, negative correlation among visibility and $PM_{2.5}$ (−0.64) and RH (−0.67). There was an exponential or power function among visibility, $PM_{2.5}$, and RH (Figure 1). The visibility decreased as $PM_{2.5}$ increased in different RH ranges. There was a threshold for the sensitivity of visibility and $PM_{2.5}$. Under

dry conditions (23% ≤ RH < 70%), the threshold of $PM_{2.5}$, corresponding to a visibility of 10 km, was 112 μg/m^3; however, under an RH of 70–80%, this threshold was lowered to 40 μg/m^3. Visibility was almost lower by 10 km when RH was 80–90%. A nonlinear correlation was observed between visibility and $PM_{2.5}$, which was affected by RH in most cases [49]. However, the relationship between visibility and $PM_{2.5}$ was not dependent on RH at higher concentrations and higher RH, because the black and red lines overlap at higher concentrations.

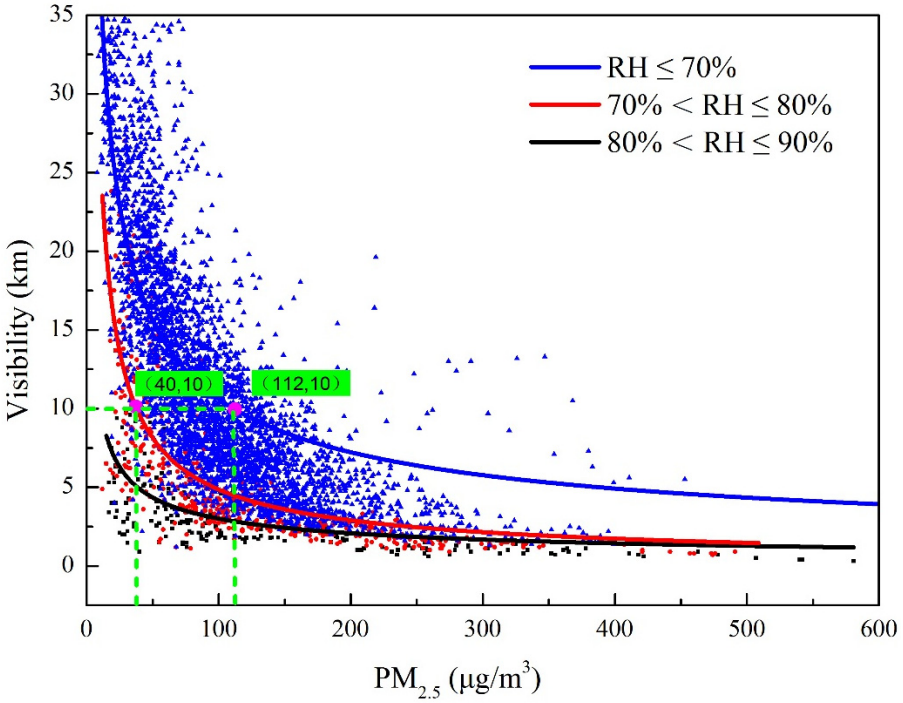

Figure 1. Variation in visibility with $PM_{2.5}$ in different RH conditions in Tianjin, 2015. Data points are colored to represent relative humidity (RH ≤ 70%, 70% < RH ≤ 80%, 80% < RH ≤ 90%); data (40 μg/m^3, 10 km) and (112 μg/m^3, 10 km) are the thresholds of $PM_{2.5}$ (40 and 112 μg/m^3) corresponding to the visibility of 10 km under the conditions of 70% < RH ≤ 80% and RH ≤ 70%.

The relationship among visibility, $PM_{2.5}$ concentration, and RH was investigated and quantified based on hourly data obtained from Tianjin, 2015, and 4453 valid datasets were used in the regression analysis (Equations (1)–(3)). The *F*-test was applied with a confidence level of 95% (α = 0.05). The regression coefficients for the three parameterization schemes are listed in Table S1 in Supplementary Materials. To test the reliability, this study compared the *V* calculated from the regression and the measured visibilities (Figure 2). The determination R^2 of Equation (3) at a confidence level of 95% was higher than that of the other two equation forms (0.72 vs. 0.55 and 0.55). The slope of measured and calculated visibility by Equation (3) (0.67) was closer to 1 than these of Equations (1) and (2) (0.55 and 0.55). This result reveals that the compound form of the power and power-exponential function can increase the accuracy of the parameterization scheme for visibility calculation (Equation (15)) in Tianjin, 2015.

$$V = f(x,y) = 166.1 \times x^{-0.56} \times (1 - y)^{0.86y} \quad (15)$$

where the visibility is a function of two parameters, $PM_{2.5}$ and RH: $f(x,y)$; *V* was the visibility, varying in the range of 0.3–34.7 km; *x* was the $PM_{2.5}$ concentration, varying in the range of 13–581 μg/m^3; and *y* was the RH, varying in the range of 4–90% in this study.

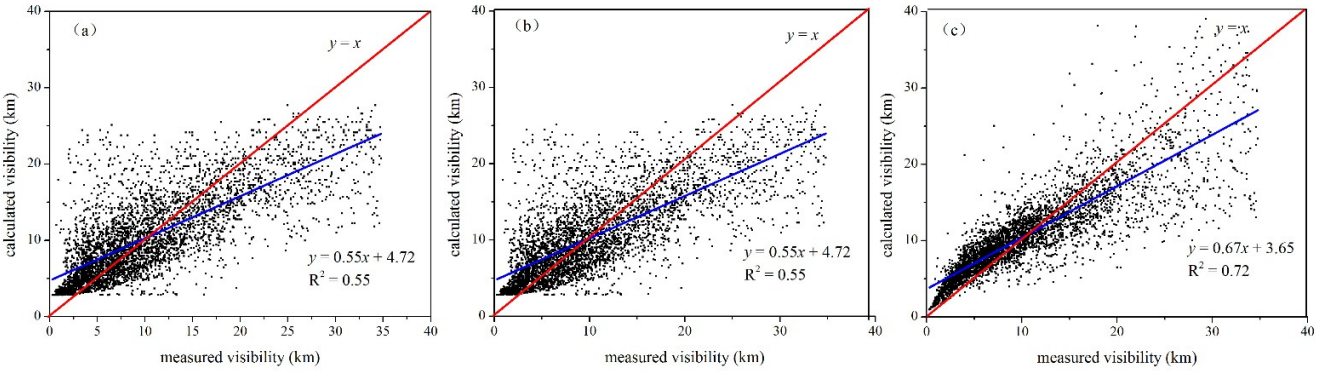

Figure 2. Comparison results calculated from regression equations and measured one-hour visibilities in Tianjin, 2015, with (**a**) 1-factor parameterization (Equation (1)) and (**b**,**c**) 2-factor parameterization (Equations (2) and (3)) at 95% confidence level; the 1:1 line is in red, and the linear fit line is blue.

3.1.2. Sensitivity of Visibility to $PM_{2.5}$ Concentration and RH

The parameterization scheme of visibility in Tianjin, 2015 (Equation (15)), was incorporated into Equations (6) and (7) (Section 2.3). At the same $PM_{2.5}$ (x_i) and RH (y_j) points, V_{x_i} was equal to V_{y_j}. The visibility relative sensitivity index ($\Omega_{PM/RH}$) in Tianjin, 2015, was calculated using Equations (16)–(18).

$$K_{V-PM2.5} = (-93.01) \times {x_i}^{-0.56} \times (1 - y_j)^{0.86\, y_j} / V_{x_i} \quad (16)$$

$$K_{V-RH} = 142.84 \times {x_i}^{-0.56} \times y_j \times (1 - y_j)^{0.86 y_j} \times [ln(1 - y_j) - y_j/(1 - y_j)]/V_{y_j} \quad (17)$$

$$\Omega_{PM/RH} = (-0.65)/\{y_j \times [ln(1 - y_j) - y_j/(1 - y_j)]\} \quad (18)$$

where V, x, and y are visibility, $PM_{2.5}$, and RH with units of km, μg/m^3, and %, respectively; x_i is the different level of $PM_{2.5}$ concentrations, i = 1, 2, 3 … … m; V_{x_i} is the visibility under the i level of $PM_{2.5}$ concentration; y_j is the different level of RH, j = 1, 2, 3 … … n; V_{y_j} is the visibility under the j level of RH; K_{V-RH} is the sensitivity index of visibility under the j level of RH; $K_{V-PM2.5}$ and K_{V-RH} is the sensitivity index of visibility to $PM_{2.5}$ concentration and RH, respectively; $\Omega_{PM/RH}$ is the ratio of visibility variation per unit of $PM_{2.5}$ to RH.

As shown in Figure 3, $\Omega_{PM/RH}$ decreased as RH increased. When RH was 45%, $\Omega_{PM/RH}$ was equal to one. The influence of $PM_{2.5}$ and RH on visibility was similar. When RH was lower than 45%, especially under 23% ($\Omega_{PM/RH}$ = 5), $\Omega_{PM/RH}$ increased sharply with the decrease in RH. Thus, visibility was mainly influenced by PM concentration, and visibility was defined as being in the $PM_{2.5}$-sensitive regime. At an RH above 75% ($\Omega_{PM/RH}$= 0.2), $\Omega_{PM/RH}$ was close to zero and did not change. It means that RH was gradually becoming the main factor influencing visibility, and visibility was identified as being in the RH-sensitive regime when RH was above 75%.

The values of 0.6, 1, 5, 10, and 15 km of visibility are the key points that refer to the classification of dense fog, fog, mist, haze, and good days. By combining Equations (15) and (18), the $PM_{2.5}$ and RH threshold values of visibility of different control categories for the above levels were determined respectively. When $\Omega_{PM/RH}$= 1, RH was 45% and $PM_{2.5}$ was 345, 100, and 48 μg/m^3, corresponding to visibility at 5, 10, and 15 km, respectively (Figure 4).

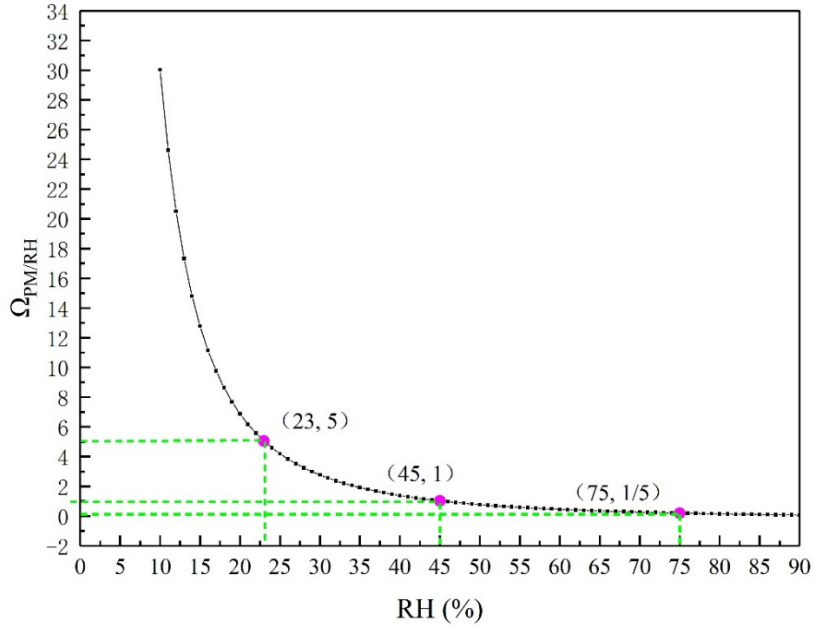

Figure 3. Variation characteristics of the visibility relative sensitivity index ($\Omega_{PM/RH}$) in Tianjin, 2015 (abscissa is RH, 10–90%; the ordinate is relative sensitivity index).

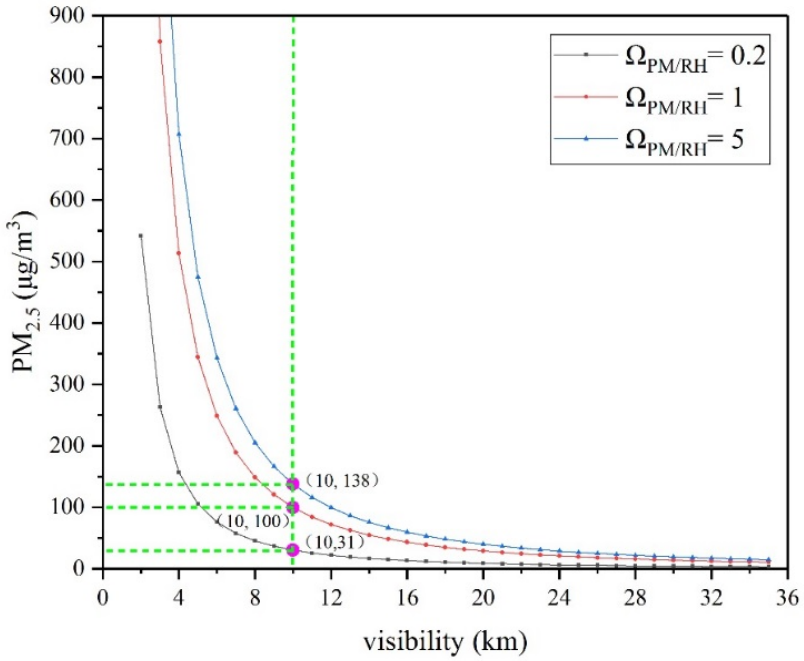

Figure 4. The $PM_{2.5}$ thresholds for different visibility-sensitive regimes ($\Omega_{PM/RH}$) = 0.2, 1, and 5, respectively) under different visibility levels in Tianjin, 2015.

When visibility was in the $PM_{2.5}$-sensitive regime ($\Omega_{PM/RH}$= 5), the threshold of RH was 23% and $PM_{2.5}$ was 475, 138, and 67 μg/m^3, corresponding to visibility at 5, 10, and 15 km, respectively. When visibility was in the RH-sensitive regime ($\Omega_{PM/RH}$= 0.2), the threshold of RH was 75% and $PM_{2.5}$ was 106, 31, and 15 μg/m^3, corresponding to visibility at 5, 10, and 15 km, respectively. When RH was >75%, visibility was more sensitive to the variation in RH than to the increase in $PM_{2.5}$. The threshold values of $PM_{2.5}$ were out of the observation values measured in this study (581 μg/m^3) at 0.6 and 1 km level of visibility,

meaning that it is hard for the contribution of particulate matter to exceed the relative humidity during dense fog and fog days.

The result shows that the classification method of visibility control categories built in this study can be used to identify the dominant factors of atmospheric visibility. The precondition was that there was a linear or nonlinear relationship among atmospheric visibility, $PM_{2.5}$, and RH, and the relationships were well fitted.

3.2. Sensitivity of Visibility to $PM_{2.5}$ Concentration and RH for Different Aerosol Types

$PM_{2.5}$ and RH were the main influencing factors on visibility, and a well-fitted parameterization scheme of visibility was provided in this study (Equation (15)). This new model could be applicable and easily transferrable to other datasets worldwide. However, there remained certain deviations between the calculated and measured visibilities (R^2 = 0.72; slope = 0.67) due to the difference in the aerosol extinction component.

3.2.1. Constituents and Extinction Characteristics of Chemical Composition in $PM_{2.5}$

Hourly concentrations of extinction compositions, such as $(NH_4)_2SO_4$, NH_4NO_3, OM, fine soil, and sea salt, were reconstructed based on Equations (10)–(14). The extinction contribution of the compositions to visibility degradation was investigated using the revised IMPROVE equation (Equation (9)). The correlation coefficient between the extinction coefficient calculated by the IMPROVE equations and visibility (Equation (19), Koschmieder's law) reached 0.88. The aerosol extinction coefficient calculated by the IMPROVE equations was highest in December (1147.4 Mm^{-1}) and lowest in June (117.0 Mm^{-1}), shown in Figure 5a. The difference was by up to 10 times. The primary extinction components were different in different months (Figure 5b). The contribution of hygroscopic compositions (NH_4NO_3, $(NH_4)_2SO_4$, and sea salt) to extinction coefficient was up to 80% in November, while it was only 46% in February. The contribution of OM to extinction was highest in February (35%), followed by October (25%), June (31%), and March (30%).

$$B_{ext} = k/V \times 1000 \quad (19)$$

where B_{ext} is the light extinction coefficient of aerosol, Mm^{-1}; V is visibility, km; and k is assumed to be 1.97 when the visibility is <10 km. Otherwise, k is assumed to be 3.912 [46,50].

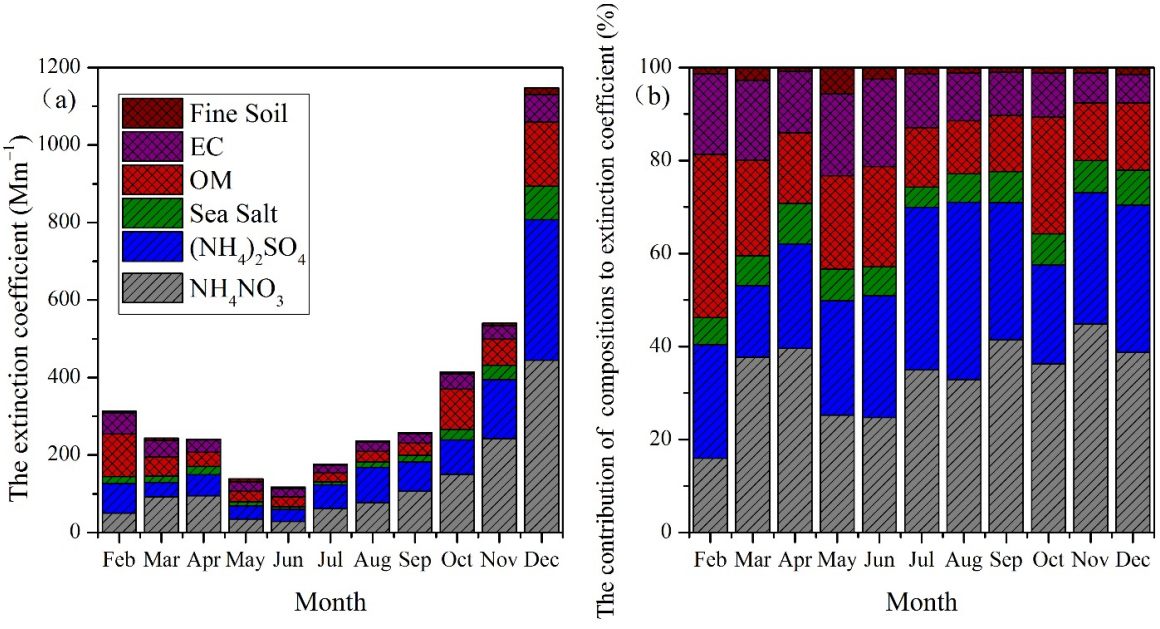

Figure 5. The monthly average extinction coefficients (**a**) and contributions (**b**) of main extinction components in $PM_{2.5}$ in Tianjin, 2015.

The annual average proportions of $(NH_4)_2SO_4$, NH_4NO_3, OM, EC, fine soil, and sea salt in $PM_{2.5}$ were 14%, 17%, 19%, 3%, 6%, and 5%, respectively. The proportions of extinction compositions in $PM_{2.5}$ changed obviously with the seasons. The monthly average proportions of extinction compositions in $PM_{2.5}$ are shown in Figure 6a. In December, November, and July, the major components accounted for the highest proportion of $PM_{2.5}$: 104%, 77%, and 68%, respectively. The proportions of major extinction compositions in $PM_{2.5}$ were lowest in February (51%) and October (51%). The content difference in the extinction component in $PM_{2.5}$ for different seasons could reach up to 2.0 times. The hygroscopic compositions of $PM_{2.5}$ accounted for the highest proportion in December (60%), followed by November (51%) and July (40%). These results suggest that constituents of the extinction composition in $PM_{2.5}$ differed by period.

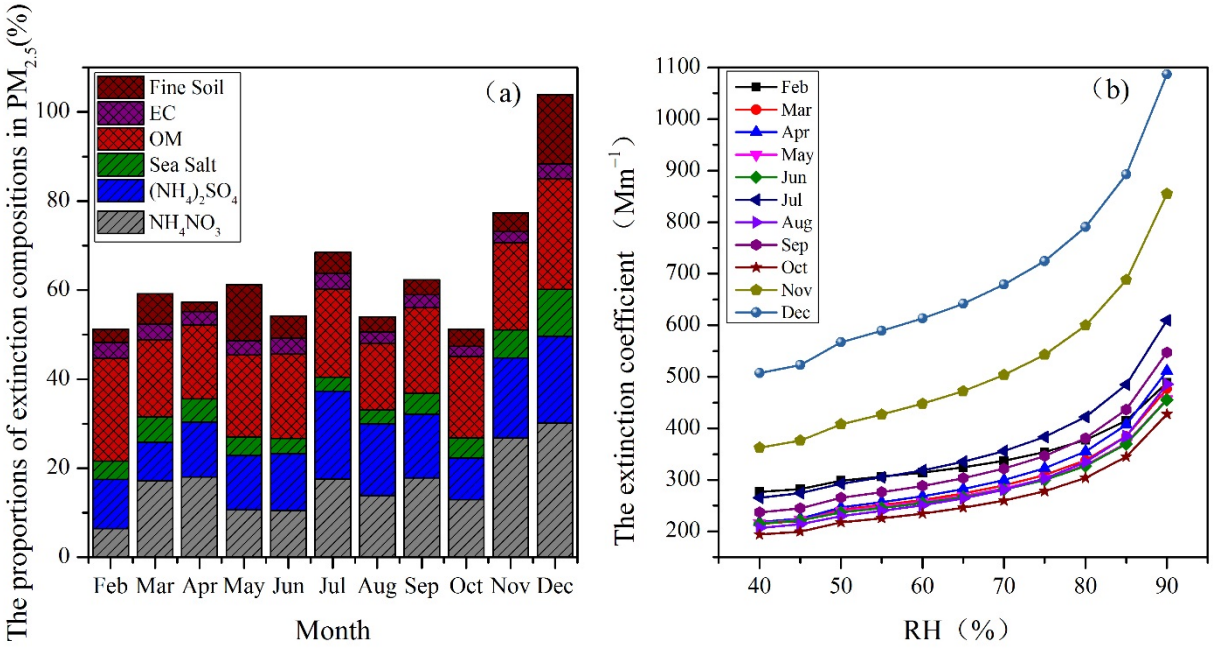

Figure 6. Monthly average proportions of major extinction compositions in $PM_{2.5}$ (**a**) and the variation of extinction coefficient with increased RH under different aerosol types, taking chemical compositions of $PM_{2.5}$ in different months for examples (**b**); chemical composition of $PM_{2.5}$ was the monthly mean proportions of extinction components in $PM_{2.5}$ in Tianjin, 2015; $PM_{2.5}$ concentration was set to 100 $\mu g/m^3$; the extinction coefficient was calculated by IMPROVE equation.

To explore the influence of composition constituents on aerosol extinction, this study used the monthly average proportions of $(NH_4)_2SO_4$, NH_4NO_3, OM, EC, fine soil, and sea salt to calculate extinction coefficients with the IMPROVE equation under the same level of $PM_{2.5}$ mass concentration (100 $\mu g/m^3$) and RH (Figure 6b). The extinction coefficients of aerosols in December were twice that of aerosols in June, even though the $PM_{2.5}$ and RH were same. This result was observed because particles with more extinction components were more efficient light scatterers and absorbers.

In February, the sum of major extinction components accounted for 53% of $PM_{2.5}$ and was similar to the 54% in August. However, the content of hygroscopic components in August (33%) was higher than that in February (22%). At low RH, the extinction coefficient in February was higher than that in March. With the increase in RH, the growth rate of the extinction coefficient in August was faster than that in February, and it was higher than that in February when RH was more than 85% (Figure 6b). The extinction coefficient of aerosol was more sensitive to RH when the content of hygroscopic components was higher.

In summary, the total content of the extinction components in the particles was the main factor affecting the extinction ability of aerosols, and the content of the hygroscopic components played a critical role in affecting their sensitivity to RH.

3.2.2. Classification of Aerosol Types

The relationships among visibility, $PM_{2.5}$, and RH depended on the extinction capacity of the aerosol composition to a certain extent. In this study, a new aerosol classification method was established based on the percentages of hygroscopic (NH_4NO_3, $(NH_4)_2SO_4$, and sea salt) and non-hygroscopic (OM, EC, and fine soil) components in $PM_{2.5}$, shown as Equations (20) and (21):

$$P_{hyg} = P_{(NH_4)_2SO_4} + P_{NH_4NO_3} + P_{SS} \quad (20)$$

$$P_{no-hyg} = P_{OM} + P_{EC} + P_{FS} \quad (21)$$

where $P_{((NH_4)_2SO_4}$, $P_{NH_4NO_3}$, P_{SS}, P_{OM}, P_{EC}, P_{FS}, P_{hyg}, and P_{no-hyg} are the percentages of NH_4NO_3, $(NH_4)_2SO_4$, sea salt, OM, EC, fine soil, hygroscopic, and non-hygroscopic extinction components in $PM_{2.5}$, respectively.

The percentages of hygroscopic and non-hygroscopic extinction components concentrated mainly on the range of 10–70% and 10–50%, shown in Figure 7. A total of 4008 aerosol samples (accounting for 90% of all samples) were classified into six types according to the numerical value of P_{hyg} and P_{no-hyg}. At the same particle concentration level, the higher the $P_{hyg} + P_{no-hyg}$ was, the more sensitive the visibility was to the change in the fine particle concentration. The higher the P_{hyg} was, the more sensitive the visibility was to the change in RH.

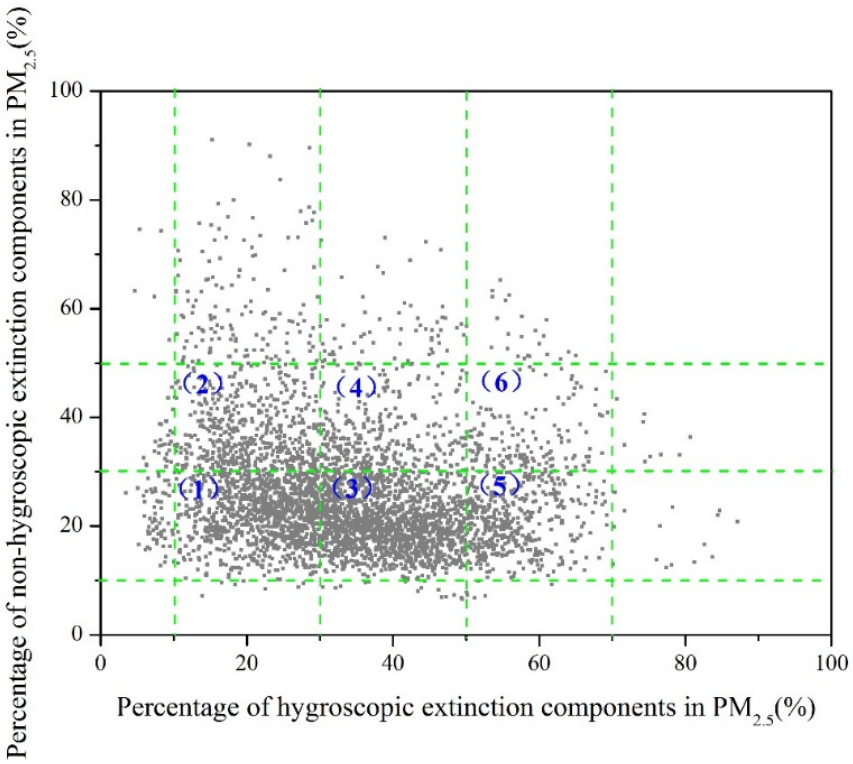

Figure 7. The percentages of hygroscopic and non-hygroscopic extinction components in $PM_{2.5}$ in Tianjin, 2015 (the numbers in brackets represent the area serial numbers for different aerosol types).

The characteristics and sample size of the six aerosol types are shown in Table S2. The sample size of aerosols with a low (types 1 and 2) and medium (types 3 and 4) content of hygroscopic components was similar, accounting for 35% and 41%, respectively. Aerosols with a high content of hygroscopic components (types 5 and 6) made up 14%. The content of non-hygroscopic extinction components (types 1, 3, and 5) in most samples (68%) was lower than 30%. Of the aerosols, 22% were in types 2, 4, and 6 with a medium content of non-hygroscopic extinction components. A good correlation between visibility and $PM_{2.5}$

was found for different aerosol types with the correlation coefficient varying from −0.54 to −0.71. The correlation coefficient between visibility and RH increased from −0.16 to −0.70 with the increase of the content of hygroscopic components.

3.2.3. Impacts of Chemical Compositions on the Sensitivity of Visibility to $PM_{2.5}$ and RH

The varied correlation among visibility, $PM_{2.5}$, and RH for different aerosol types indicated that the content of chemical compositions greatly influences the sensitivity of visibility to $PM_{2.5}$ and RH. In this study, the quantitative relationship among visibility, PM concentration, and RH in different aerosol types was fitted based on Equations (1)–(3).FS The compound form of the power and power-exponential function was still identified as the optimal fit among visibility, $PM_{2.5}$, and RH (Equation (3)). Coefficients and fitting effects varied by aerosol type (Table 1). The calculated visibility for types 1, 2, and 4 fitted the measured visibility less effectively; R^2 was 0.65, 0.66, and 0.64, respectively. The R^2 between the measured and calculated visibility in aerosols with high hygroscopic and low non-hygroscopic content (types 3, 5, and 6) was above 0.76. The linear slopes of correlation between calculated and measured visibility were higher (0.72–0.84) in types 3, 5, and 6 than in other types. The fitting equation for types 3, 5, and 6 increased the accuracy of the parameterization scheme for visibility calculation.

Table 1. Fitting equation and effect of visibility, $PM_{2.5}$, and RH for different aerosol types.

Type	Fitting Equation	Relationship between Measured and Calculated Visibility	R^2
1	$V = 447.9 \times [PM_{2.5}]^{-0.77} \times (1 - RH)^{0.67 \cdot RH}$	$y = 0.62x + 4.66$	0.65
2	$V = 159.4 \times [PM_{2.5}]^{-0.55} \times (1 - RH)^{0.42 \cdot RH}$	$y = 0.64x + 5.83$	0.66
3	$V = 496.6 \times [PM_{2.5}]^{-0.82} \times (1 - RH)^{0.99 \cdot RH}$	$y = 0.75x + 1.93$	0.76
4	$V = 176.7 \times [PM_{2.5}]^{-0.59} \times (1 - RH)^{0.72 \cdot RH}$	$y = 0.61x + 4.58$	0.64
5	$V = 491.9 \times [PM_{2.5}]^{-0.85} \times (1 - RH)^{1.08 \cdot RH}$	$y = 0.84x + 0.65$	0.84
6	$V = 132.4 \times [PM_{2.5}]^{-0.51} \times (1 - RH)^{1.04 \cdot RH}$	$y = 0.72x + 1.90$	0.76
annual	$V = 166.1 \times [PM_{2.5}]^{-0.56} \times (1 - RH)^{0.86 \cdot RH}$	$y = 0.67x + 3.65$	0.72

Based on the division method of visibility control categories established in Section 2.3, the thresholds for identifying the $PM_{2.5}$-sensitive regime and RH-sensitive regime under different aerosol types were determined (Figure 8).

The $PM_{2.5}$ and RH thresholds of varied visibility-sensitive regimes differed with aerosol types. When visibility was 10 km, the $PM_{2.5}$-sensitive regime was identified by RH < 30%, 31%, 26%, 26%, 25%, and 20% and $PM_{2.5}$ > 129, 141, 106, 117, 91, and 146 $\mu g/m^3$ in types 1–6, respectively. The RH-sensitive regime was characterized by RH > 83%, 85%, 79%, 78%, 78%, and 70% and by $PM_{2.5}$ < 40, 45, 26, 30, 22, and 29 $\mu g/m^3$ in types 1–6, respectively. Other visibility control categories were classified into transition regimes dominated by $PM_{2.5}$ and RH with RH = 56%, 58%, 50%, 49%, 49%, and 41% and $PM_{2.5}$ = 95, 105, 77, 86, 65, and 103 $\mu g/m^3$, respectively. The threshold difference of $PM_{2.5}$ was by up to 1.6 times.

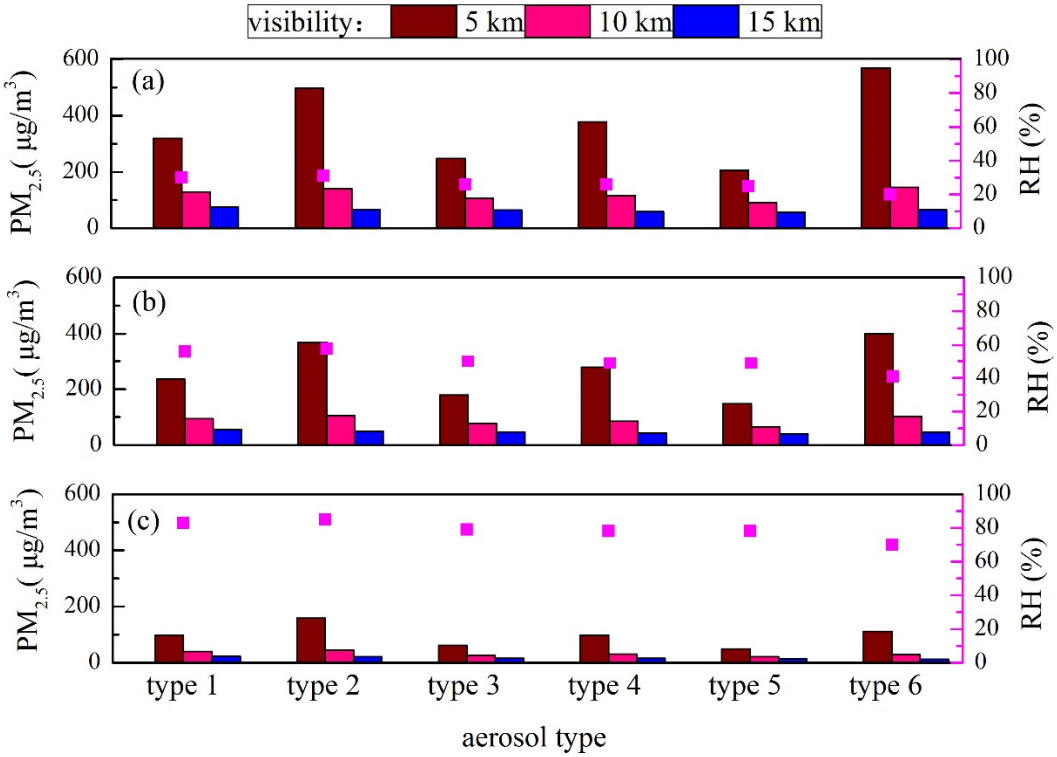

Figure 8. $PM_{2.5}$ (the histogram) and RH (the pink scatter) threshold values of visibility-sensitive regimes for aerosol types in Tianjin, 2015 (**a**–**c** are the values with a relative sensitivity index ($\Omega_{PM/RH}$) = 5, 1, and 0.2, respectively).

According to the threshold values of the visibility control categories, the proportion of those in different types in Tianjin, 2015, is shown in Table 2. The proportion of transition regimes dominated by $PM_{2.5}$ in type 1 was up to 48%, and that of transition regimes dominated by RH was 23%. The proportion of transition regimes dominated by $PM_{2.5}$ was still dominant (47%) in type 2. The proportions of the $PM_{2.5}$-sensitive regime (47%) in type 2 were higher than those of the other types. The proportions of the transition regimes dominated by $PM_{2.5}$ and RH were similar (31% vs. 31% and 59% vs. 54%, respectively) in types 3 and 4. The transition regime dominated by RH became prominent in types 5 and 6 (77% and 46%). The proportions of the RH-sensitive regime were higher than those of other types in type 6 (44%).

Table 2. Proportion of different visibility-sensitive regimes under varied aerosol types in Tianjin, 2015 (%).

Aerosol Types	$PM_{2.5}$-Sensitive Regime	Transition Regime Dominated by $PM_{2.5}$	Transition Regime Dominated by RH	RH-Sensitive Regime
1	27	48	23	2
2	47	47	6	0
3	6	31	59	3
4	9	31	54	6
5	1	13	77	9
6	3	8	46	44
annual	13	31	47	9

4. Conclusions

Many previous studies were performed to explore the complex relationships among visibility, $PM_{2.5}$ concentration, and RH. However, the relative contribution of the two fac-

tors to visibility degradation, especially for different aerosol types, was difficult to quantify. The impact of chemical compositions on the sensitivity of visibility to $PM_{2.5}$ and RH was explored based on the online monitoring data of RH, visibility, $PM_{2.5}$, and its major components in this study. The normalized forward sensitivity index method for identifying the dominant factors of visibility was used based on the functional equation among visibility, RH, and $PM_{2.5}$ mass concentration given different aerosol types. Visibility was identified as being in the $PM_{2.5}$- or RH-sensitive regime according to the corresponding threshold.

The method was verified and evaluated in Tianjin. There was a compound relationship of the power and power-exponential functions among visibility, $PM_{2.5}$, and RH. The R^2 between the calculated and measured visibilities reached 0.72, and the slope was 0.67. Visibility was identified as being in the $PM_{2.5}$-sensitive or RH-sensitive regime. Corresponding thresholds of $PM_{2.5}$ were determined by function among visibility, $PM_{2.5}$, and RH. Chemical compositions ($(NH_4)_2SO_4$, NH_4NO_3, OC, EC, fine soil, and sea salt) influenced the sensitivity of visibility to $PM_{2.5}$ and RH due to varying degrees of dry extinction efficiency and hygroscopicity. A good correlation between visibility and $PM_{2.5}$ was found for different aerosol types with the correlation coefficient varying from -0.54 to -0.71. The correlation coefficient between visibility and RH changed from -0.16 to -0.70 with the increase of the content of hygroscopic components. The results showed that the normalized forward sensitivity index method is suitable for various aerosol types and can be applied to identify the leading factors of atmospheric visibility decline as long as synchronous, high-resolution data of visibility, $PM_{2.5}$, and RH are collected. However, for different aerosol types, the $PM_{2.5}$ thresholds under the same visibility-sensitive regimes can be several times different, while the RH threshold changes gently. The thresholds for different aerosol types obtained in this study can be used as a reference for other cities with the data of extinction component content in $PM_{2.5}$. Next, we will further evaluate the applicability of the method in other cities.

Supplementary Materials: The following supporting information can be downloaded at: https://www.mdpi.com/article/10.3390/atmos13030471/s1; Table S1: Summary of regression coefficients for the Equations (1)–(3) parameterization schemes at 95 % confidence level (α = 0.05); Table S2: Characteristics and sample size of six aerosol types in Tianjin 2015

Author Contributions: Conceptualization, Y.Z. and Y.F.; Data curation, J.W. (Jiao Wang), J.W. (Jianhui Wu) and S.H.; Formal analysis, B.L., X.L. and H.G.; Funding acquisition, J.W. (Jianhui Wu) and S.H.; Investigation, X.L.; Methodology, J.W. (Jiao Wang), Y.Z. and X.G.; Resources, Y.F.; Validation, X.G.; Visualization, B.L.; Writing—original draft, J.W. (Jiao Wang) and J.W. (Jianhui Wu); Writing—review and editing, H.G. and Y.Z. All authors have read and agreed to the published version of the manuscript.

Funding: This research was funded by Suqin Han grant number 41771242 and Jianhui Wu grant number 18ZXSZSF00160.

Institutional Review Board Statement: Not applicable.

Informed Consent Statement: Not applicable.

Data Availability Statement: Restrictions apply to the availability of these data. Data was obtained from the Tianjin Eco-Environmental Monitoring Center and Tianjin Environmental Meteorological Center, and are available from the authors with the permission of the Tianjin Eco-Environmental Monitoring Center and Tianjin Environmental Meteorological Center.

Acknowledgments: This research was funded by the National Natural Science Foundation of China (grant number 41771242) and the Tianjin Science and Technology Foundation (grant number 18ZXSZSF00160). We would like to thank the Tianjin Eco-Environmental Monitoring Center and Tianjin Environmental Meteorological Center for their support.

Conflicts of Interest: The authors declare no conflict of interest.

References

1. Watson, J.G. Critical review discussion-visibility, Science and regulation. *J. Air Waste Manag. Assoc.* **2002**, *52*, 973–999. [CrossRef]
2. Doyle, M.; Dorling, S. Visibility trends in the UK 1950–1997. *Atmos. Environ.* **2002**, *36*, 3161–3172. [CrossRef]
3. Hu, Y.; Yao, L.; Cheng, Z.; Wang, Y. Long-term atmospheric visibility trends in megacities of China, India and the United States. *Environ. Res.* **2017**, *159*, 466–473. [CrossRef] [PubMed]
4. Li, J.; Li, C.; Zhao, C.; Su, T. Changes in surface aerosol extinction trends over China during 1980–2013 inferred from quality-controlled visibility data. *Geophys. Res. Lett.* **2016**, *43*, 8713–8719. [CrossRef]
5. Zhang, F.; Xu, L.; Chen, J.; Yu, Y.; Niu, Z.; Yin, L. Chemical compositions and extinction coefficients of PM2.5 in peri-urban of Xiamen, China, during June 2009–May 2010. *Atmos. Res.* **2012**, *106*, 150–158. [CrossRef]
6. Founda, D.; Kazadzis, S.; Mihalopoulos, N.; Gerasopoulos, E.; Lianou, M.; Raptis, P.I. Long-term visibility variation in Athens (1931–2013): A proxy for local and regional atmospheric aerosol loads. *Atmos. Chem. Phys.* **2016**, *16*, 11219–11236. [CrossRef]
7. Han, L.; Sun, Z.; He, J.; Hao, Y.; Tang, Q.; Zhang, X.; Zheng, C.; Miao, S. Seasonal variation in health impacts associated with visibility in Beijing, China. *Sci. Total Environ.* **2020**, *730*, 139149. [CrossRef]
8. Singh, A.; Dey, S. Influence of aerosol composition on visibility in megacity Delhi. *Atmos. Environ.* **2012**, *62*, 367–373. [CrossRef]
9. Shen, X.; Sun, J.; Zhang, X.; Zhang, Y.; Zhang, L.; Che, H.; Ma, Q.; Yu, X.; Yue, Y. Characterization of submicron aerosols and effect on visibility during a severe haze-fog episode in Yangtze River Delta, China. *Atmos. Environ.* **2015**, *120*, 307–316. [CrossRef]
10. Singh, A.; Bloss, W.J.; Pope, F.D. 60 years of UK visibility measurements: Impact of meteorology and atmospheric pollutants on visibility. *Atmos. Chem. Phys.* **2017**, *17*, 2085–2101. [CrossRef]
11. Cao, J.-J.; Wang, Q.-Y.; Chow, J.C.; Watson, J.; Tie, X.-X.; Shen, Z.-X.; Wang, P.; An, Z.-S. Impacts of aerosol compositions on visibility impairment in Xi'an, China. *Atmos. Environ.* **2012**, *59*, 559–566. [CrossRef]
12. Shen, Z.X.; Cao, J.J.; Arimoto, R.; Han, Z.; Zhang, R.; Han, Y.; Liu, S.; Okuda, T.; Nakao, S.; Tanaka, S. Ionic composition of TSP and $PM_{2.5}$ during dust storms and air pollution episodes at Xi'an, China. *Atmos. Environ.* **2009**, *43*, 2911–2918. [CrossRef]
13. Wang, H.; Xu, J.; Zhang, M.; Yang, Y.; Shen, X.; Wang, Y.; Chen, D.; Guo, J. A study of the meteorological causes of a prolonged and severe haze episode in January 2013 over central-eastern China. *Atmos. Environ.* **2014**, *98*, 146–157. [CrossRef]
14. Zhang, Q.; Quan, J.N.; Tie, X.X.; Li, X.; Liu, Q.; Gao, Y.; Zhao, D.L. Effects of meteorology and secondary particle formation on visibility during heavy haze events in Beijing, China. *Sci. Total Environ.* **2015**, *502*, 578–584. [CrossRef] [PubMed]
15. Luan, T.; Guo, X.L.; Guo, L.J.; Zhang, T. Quantifying the relationship between $PM_{2.5}$ concentration, visibility and planetary boundary layer height for long-lasting haze and fog-haze mixed events in Beijing. *Atmos. Chem. Phys.* **2018**, *18*, 203–225. [CrossRef]
16. Zhao, P.; Zhang, X.; Xu, X.; Zhao, X. Long-term visibility trends and characteristics in the region of Beijing, Tianjin, and Hebei, China. *Atmos. Res.* **2011**, *101*, 711–718. [CrossRef]
17. Huang, K.; Zhuang, G.; Lin, Y.; Wang, Q.; Fu, J.S.; Zhang, R.; Li, J.; Deng, C.; Fu, Q. Impact of anthropogenic emission on air quality over a megacity-revealed from an intensive atmospheric campaign during the Chinese Spring Festival. *Atmos. Chem. Phys.* **2012**, *12*, 11631–11645. [CrossRef]
18. Kong, L.; Xin, J.; Liu, Z.; Zhang, K.; Tang, G.; Zhang, W.; Wang, Y. The $PM_{2.5}$ threshold for aerosol extinction in the Beijing megacity. *Atmos. Environ.* **2017**, *167*, 458–465. [CrossRef]
19. Wang, X.; Zhang, R.; Yu, W. The Effects of $PM_{2.5}$ Concentrations and Relative Humidity on Atmospheric Visibility in Beijing. *J. Geophys. Res. Atmos.* **2019**, *124*, 2235–2259. [CrossRef]
20. Deng, H.; Tan, H.; Li, F.; Cai, M.; Chan, P.W.; Xu, H.; Huang, X.; Wu, D. Impact of relative humidity on visibility degradation during a haze event: A case study. *Sci. Total Environ.* **2016**, *569–570*, 1149–1158. [CrossRef]
21. Malm, W.C.; Day, D.E. Estimates of aerosol species scattering characteristics as a function of relative humidity. *Atmos. Environ.* **2001**, *35*, 2845–2860. [CrossRef]
22. Chen, J.; Zhao, C.S.; Ma, N.; Liu, P.F.; Göbel, T.; Hallbauer, E.; Deng, Z.Z.; Ran, L.; Xu, W.Y.; Liang, Z.; et al. A parameterization of low visibilities for hazy days in the North China Plain. *Atmos. Chem. Phys.* **2012**, *12*, 4935–4950. [CrossRef]
23. Wu, Y.; Wang, X.; Yan, P.; Zhang, L.; Tao, J.; Liu, X.; Tian, P.; Han, Z.; Zhang, R. Investigation of hygroscopic growth effect on aerosol scattering coefficient at a rural site in the southern North China Plain. *Sci. Total Environ.* **2017**, *599–600*, 76–84. [CrossRef]
24. Covert, D.S.; Charlson, R.J.; Ahlquist, N.C. A Study of the Relationship of Chemical Composition and Humidity to Light Scattering by Aerosols. *J. Appl. Meteorol.* **1972**, *11*, 968–976. [CrossRef]
25. Li, Y.; Huang, H.X.; Griffith, S.M.; Wu, C.; Lau, A.K.; Yu, J.Z. Quantifying the relationship between visibility degradation and $PM_{2.5}$ constituents at a suburban site in Hong Kong: Differentiating contributions from hydrophilic and hydrophobic organic compounds. *Sci. Total Environ.* **2017**, *575*, 1571–1581. [CrossRef] [PubMed]
26. Wen, C.-C.; Yeh, H.-H. Comparative influences of airborne pollutants and meteorological parameters on atmospheric visibility and turbidity. *Atmos. Res.* **2010**, *96*, 496–509. [CrossRef]
27. Schichtel, B.A.; Husar, R.B.; Falke, S.R.; Wilson, W.E. Haze trends over the United States, 1980–1995. *Atmos. Environ.* **2001**, *35*, 5205–5210. [CrossRef]
28. Sun, Y.; Chen, C.; Zhang, Y.; Xu, W.; Zhou, L.; Cheng, X.; Zheng, H.; Ji, D.; Li, J.; Tang, X.; et al. Rapid formation and evolution of an extreme haze episode in Northern China during winter 2015. *Sci. Rep.* **2016**, *6*, 27151. [CrossRef] [PubMed]
29. Day, D.E.; Malm, W.C. Aerosol light scattering measurements as a function of relative humidity: A comparison between measurements made at three different sites. *Atmos. Environ.* **2001**, *35*, 5169–5176. [CrossRef]

30. Wang, B.; Chen, Y.; Zhou, S.; Li, H.; Wang, F.; Yang, T. The influence of terrestrial transport on visibility and aerosol properties over the coastal East China Sea. *Sci. Total Environ.* **2018**, *649*, 652–660. [CrossRef] [PubMed]
31. Tao, J.; Zhang, L.; Engling, G.; Zhang, R.; Yang, Y.; Cao, J.; Zhu, C.; Wang, Q.; Luo, L. Chemical composition of $PM_{2.5}$ in an urban environment in Chengdu, China: Importance of springtime dust storms and biomass burning. *Atmos. Res.* **2012**, *122*, 270–283. [CrossRef]
32. Ye, B.M.; Ji, X.L.; Yang, H.Z.; Yao, X.; Chan, K.C.; Cadle, S.H.; Chan, T.; Mulawa, P.A. Concentration and chemical composition of $PM_{2.5}$ in Shanghai for a 1-year period. *Atmos. Environ.* **2003**, *37*, 499–510. [CrossRef]
33. Ma, N.; Zhao, C.; Chen, J.; Xu, W.; Yan, P.; Zhou, X. A novel method for distinguishing fog and haze based on $PM_{2.5}$, visibility, and relative humidity. *Sci. China Earth Sci.* **2014**, *57*, 2156–2164. [CrossRef]
34. Liu, B.; Yang, J.; Yuan, J.; Wang, J.; Dai, Q.; Li, T.; Bi, X.; Feng, Y.; Xiao, Z.; Zhang, Y.; et al. Source apportionment of atmospheric pollutants based on the online data by using PMF and ME2 models at a megacity, China. *Atmos. Res.* **2017**, *185*, 22–31. [CrossRef]
35. Li, Y.F.; Liu, B.S.; Xue, Z.G.; Zhang, Y.F. Chemical characteristics and source apportionment of $PM_{2.5}$ using PMF modelling coupled with 1-h resolution online air pollutant dataset for Linfen, China. *Environ. Pollut.* **2020**, *263*, 114532. [CrossRef]
36. Song, M.; Han, S.Q.; Zhang, M.; Yao, Q.; Zhu, B. Relationship between visibility and relative humidity, PM_{10}, $PM_{2.5}$ in Tianjin. *J. Meteor. Environ.* **2013**, *29*, 34–41. (In Chinese)
37. Randriamiarisoa, H.; Chazette, P.; Couvert, P.; Sanak, J.; Mégie, G. Relative humidity impact on aerosol parameters in a Paris suburban area. *Atmos. Chem. Phys.* **2006**, *6*, 1389–1407. [CrossRef]
38. Carrico, C.M.; Rood, M.J.; Ogren, J.A.; Neusüss, C.; Wiedensohler, A.; Heintzenberg, J.; Neusüß, C. Aerosol Optical properties at Sagres, Portugal during ACE-2. *Tellus B Chem. Phys. Meteorol.* **2000**, *52*, 694–715. [CrossRef]
39. Chitnis, N.; Hyman, J.; Cushing, J. Determining Important Parameters in the Spread of Malaria through the Sensitivity Analysis of a Mathematical Model. *Bull. Math. Biol.* **2008**, *70*, 1272–1296. [CrossRef] [PubMed]
40. Aguilar-Canto, F.J.; de León, U.A.-P.; Avila-Vales, E. Sensitivity theorems of a model of multiple imperfect vaccines for COVID-19. *Chaos Solitons Fractals* **2022**, *156*, 111844. [CrossRef] [PubMed]
41. Malm, W.C.; Gebhart, K.A.; Molenar, J.; Cahill, T.; Eldred, R.; Huffman, D. Examining the relationship between atmospheric aerosols and light extinction at Mount-Rainier-National-Park and North-Cascades-National-Park. *Atmos. Environ.* **1994**, *28*, 347–360. [CrossRef]
42. Pitchford, M.; Malm, W.; Schichtel, B.; Kumar, N.; Lowenthal, D.; Hand, J. Revised algorithm for estimating light extinction from IMPROVE particle speciation data. *J. Air Waste Manag. Assoc.* **2007**, *57*, 1326–1336. [CrossRef] [PubMed]
43. Wang, J.; Zhang, Y.-F.; Feng, Y.-C.; Zheng, X.-J.; Jiao, L.; Hong, S.-M.; Shen, J.-D.; Zhu, T.; Ding, J.; Zhang, Q. Characterization and source apportionment of aerosol light extinction with a coupled model of CMB-IMPROVE in Hangzhou, Yangtze River Delta of China. *Atmos. Res.* **2016**, *178–179*, 570–579. [CrossRef]
44. Wang, Q.; Sun, Y.; Jiang, Q.; Du, W.; Sun, C.; Fu, P.; Wang, Z. Chemical composition of aerosol particles and light extinction apportionment before and during the heating season in Beijing, China. *J. Geophys. Res. Atmos.* **2015**, *120*, 12708–12722. [CrossRef]
45. Turpin, B.J.; Lim, H.J. Species Contributions to $PM_{2.5}$ Mass Concentrations: Revisiting Common Assumptions for Estimating Organic Mass. *Aerosol. Sci. Technol.* **2001**, *35*, 602–610. [CrossRef]
46. Zou, J.; Liu, Z.; Hu, B.; Huang, X.; Wen, T.; Ji, D.; Liu, J.; Yang, Y.; Yao, Q.; Wang, Y. Aerosol chemical compositions in the North China Plain and the impact on the visibility in Beijing and Tianjin. *Atmos. Res.* **2018**, *201*, 235–246. [CrossRef]
47. Tao, J.; Zhang, L.; Gao, J.; Wang, H.; Chai, F.; Wang, S. Aerosol chemical composition and light scattering during a winter season in Beijing. *Atmos. Environ.* **2015**, *110*, 36–44. [CrossRef]
48. Aldabe, J.; Elustondo, D.; Santamaría, C.; Lasheras, E.; Pandolfi, M.; Alastuey, A.; Querol, X.; Santamaría, J.M. Chemical characterisation and source apportionment of $PM_{2.5}$ and PM_{10} at rural, urban and traffic sites in Navarra (North of Spain). *Atmos. Res.* **2011**, *102*, 191–205. [CrossRef]
49. Fu, X.; Wang, X.; Hu, Q.; Li, G.; Ding, X.; Zhang, Y.; He, Q.; Liu, T.; Zhang, Z.; Yu, Q.; et al. Changes in visibility with $PM_{2.5}$ composition and relative humidity at a background site in the Pearl River Delta region. *J. Environ. Sci.* **2016**, *40*, 10–19. [CrossRef] [PubMed]
50. Yu, X.; Ma, J.; An, J.; Yuan, L.; Zhu, B.; Liu, D.; Wang, J.; Yang, Y.; Cui, H. Impacts of meteorological condition and aerosol chemical compositions on visibility impairment in Nanjing, China. *J. Clean. Prod.* **2016**, *131*, 112–120. [CrossRef]